

Communication

# All-Polarization-Maintaining, Mode-Locking Fiber Front-End Laser Delivering Both the Picosecond Seed Laser and the Femtosecond Seed Laser

Yinuo Zhang <sup>1</sup>, Hao Zhang <sup>1</sup>, Kong Gao <sup>2</sup>, Wenchao Qiao <sup>1,2,3</sup>, Tianli Feng <sup>1,2,3</sup>, Xian Zhao <sup>2,3</sup> and Yizhou Liu <sup>1,2,3,\*</sup>

<sup>1</sup> School of Information Science and Engineering and Shandong Provincial Key Laboratory of Laser Technology and Application, Shandong University, Qingdao 266237, China

<sup>2</sup> Key Laboratory of Laser & Infrared System, Ministry of Education, Shandong University, Qingdao 266237, China

<sup>3</sup> Center for Optics Research and Engineering, Shandong University, Qingdao 266237, China

\* Correspondence: yizhou.liu@sdu.edu.cn

**Abstract:** An ytterbium-doped, mode-locking fiber front-end laser, delivering both a femtosecond seed laser and picosecond seed laser, was demonstrated. The fundamental repetition rate of the 1031 nm mode-locked laser was 32.77 MHz, realized with the all-polarization-maintaining (all-PM) nonlinear amplifying loop mirror (NALM). The femtosecond seed laser and the picosecond seed laser were delivered after carefully optimizing the nonlinear amplification process. The corresponding pulse durations were 85 fs and 2.88 ps, with average power of 171 mW and 562.5 mW, respectively.

**Keywords:** fiber laser; nonlinear amplifying loop mirror; nonlinear amplification



**Citation:** Zhang, Y.; Zhang, H.; Gao, K.; Qiao, W.; Feng, T.; Zhao, X.; Liu, Y. All-Polarization-Maintaining, Mode-Locking Fiber Front-End Laser Delivering Both the Picosecond Seed Laser and the Femtosecond Seed Laser. *Photonics* **2023**, *10*, 665. <https://doi.org/10.3390/photronics10060665>

Received: 14 May 2023

Revised: 5 June 2023

Accepted: 6 June 2023

Published: 8 June 2023



**Copyright:** © 2023 by the authors. Licensee MDPI, Basel, Switzerland. This article is an open access article distributed under the terms and conditions of the Creative Commons Attribution (CC BY) license (<https://creativecommons.org/licenses/by/4.0/>).

## 1. Introduction

In the past few decades, ultrafast fiber lasers with picosecond- or femtosecond-level pulse durations have been developed as the advanced laser sources for multiple applications, such as multiphoton microscopy [1,2], optical communication [3,4], micromachining [5,6], harmonic generation [7–9], terahertz generation with Bessel profile [10], and optical dynamics of the soliton laser [11–13]. Many contributions were implemented in investigating the optical characteristics of ultrafast fiber lasers. In 2015, C. Li et al. demonstrated a 600 mW, 64 fs, 1  $\mu\text{m}$  Yb-doped mode-locking fiber laser with the highest recorded fundamental repetition rate of 1 GHz [14]. In 2017, Z. Liu et al. built a ring-cavity Mamyshev oscillator, delivering 40 fs,  $\sim 17$  MHz, 1  $\mu\text{m}$  mode-locking pulses with  $\sim 1$  MW peak power [15]. Further, in 2010, a 1.2 W, 120 fs, 65.3 MHz, 1  $\mu\text{m}$  mode-locking laser realized with a large-pitch photonic crystal fiber was reported by Y. Song et al. [16].

The efforts in developing ultrafast laser sources delivering both a femtosecond seed laser and a picosecond seed laser are proved to be attractive for multiple state-of-the-art applications, such as the optical synchronization for high-intensity laser facility [17,18], X-ray optics [19], beam synchronous timing system for nuclear research [20], and mid-infrared optical parametric chirped pulse amplification (OPCPA) [21,22]. The delivered femtosecond seed laser and picosecond seed laser can be operated under the passively timing-linked status. Therefore, expensive actively timing-linked modules are no longer necessary. The robustness of the subsequent hybrid optical system built with the passively timing-linked seed laser can be significantly improved with higher compactness and lower costs.

The ultrafast polarization-maintaining (PM) fiber oscillator delivering both the femtosecond seed laser and the picosecond seed laser can be realized by utilizing the mode-locking mechanism of the nonlinear amplifying loop mirror (NALM) [23,24]. A 60 mW, 93 fs, 6 MHz, 1  $\mu\text{m}$ , all-PM NALM laser was realized by Y. Yu et al. in 2018 [25]. In 2017, G. Liu et al. demonstrated the NALM-based Yb-doped fiber laser delivering the 51 mW, 84 fs, 500 MHz, 1  $\mu\text{m}$  mode-locking pulses [26]. A 104 mW, 44.6 fs, 257 MHz, 1550 nm

mode-locked NALM laser was reported by W. Gao et al. in 2018 [27]. However, to date, all-PM fiber front-end lasers delivering both the picosecond seed laser and the femtosecond seed laser are rarely reported.

Utilizing the NALM with the all-normal dispersion fiber cavity, the significant optical spectrum evolution of the mode-locking pulses can be realized. The generation of the picosecond seed laser can be ensured after introducing the narrow-band optical band-pass filter into the linear arm of the NALM laser [28]. Based on the efforts of the all-normal net-cavity dispersion and the optical characteristics of the NALM [29], the femtosecond seed laser can be delivered via the transmission port of the NALM. The subsequent nonlinear fiber amplifiers are also necessary in optimizing the optical performances of the delivered picosecond seed laser and the femtosecond seed laser.

In this letter, we built an all-PM fiber front-end laser delivering both the picosecond seed laser and the femtosecond seed laser. The 562.5 mW, 2.88-ps, 32.77 MHz, and 1032.5 nm mode-locking pulses were achieved, after amplifying the signal pulses delivered by the reflection port of the NALM. The 171 mW, 85 fs, 32.77 MHz, 1029 nm mode-locking pulses were achieved by applying the double-pass nonlinear amplification. Further detailed experiments were also conducted in optimizing the optical nonlinear evolution of the delivered laser pulses. The measured root mean square (RMS) of the attenuated output powers of the femtosecond seed laser and the picosecond seed laser was 0.06% and 0.11%, respectively. The experimental results indicate that this home-built all-PM fiber front-end laser can be utilized in satisfying the urgent requirements of the aforementioned state-of-the-art applications.

## 2. Experimental Setup

Figure 1 illustrates a schematic construction of the all-PM fiber front-end laser, consisting of the nonlinear amplifying loop mirror (NALM) oscillator, the picosecond laser delivering stage, and the femtosecond laser delivering stage. The NALM oscillator consists of an 80:20 PM fiber coupler, 0.5 m PM Yb-doped gain fiber (INO, Yb-401 PM), a PM fiber WDM, a 976 nm laser diode, and  $\pi/2$  phase bias with PM fiber pigtails. The transmission port was utilized to emit the femtosecond mode-locking laser. The 2.64 mW, 1031 nm signal laser was delivered via the transmission port of the NALM laser under pump power of 68 mW. The linear arm of the NALM oscillator was composed of the reflection port of the NALM, the 2.6 nm PM fiber band-pass filter, and the 95:5 output coupler (OC). The 0.155 mW, 32.77 MHz, 1031.5 nm signal laser was delivered by the OC.

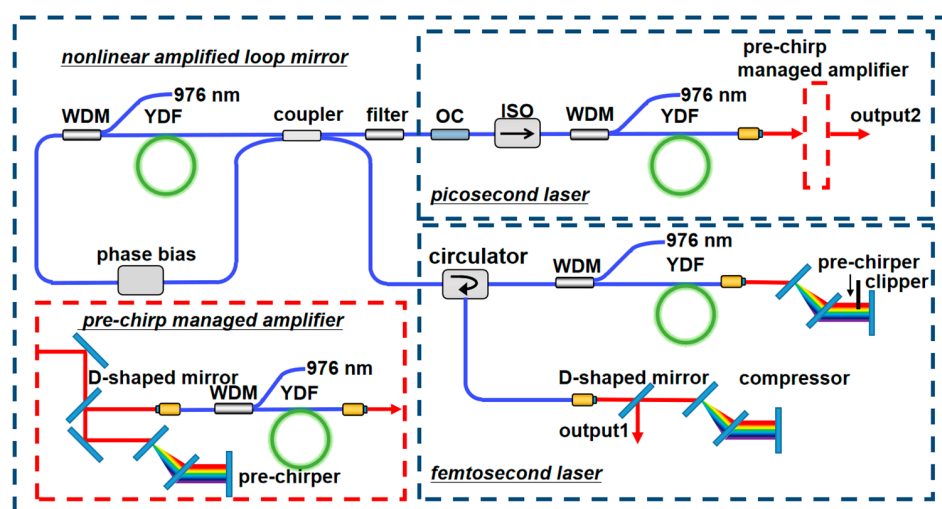


**Figure 1.** Schematic construction of the all-PM fiber front-end laser. The pre-chirp managed amplifier of the picosecond laser delivering stage is illustrated in the red rectangle dashed line. WDM, wavelength division multiplexer; ISO, isolator; OC, output coupler; YDF, ytterbium-doped fiber.

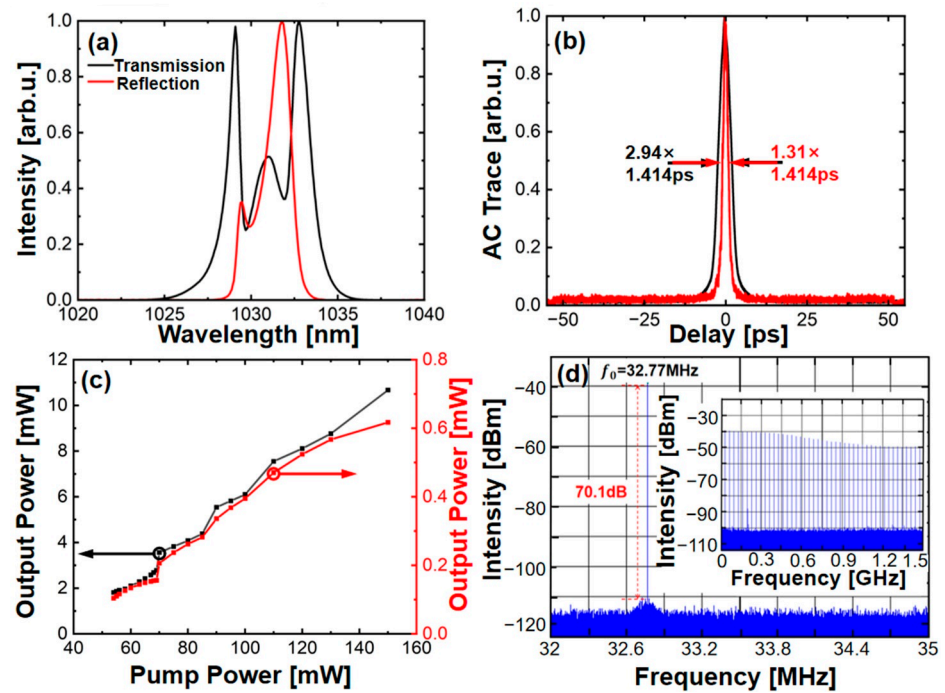
The femtosecond laser delivering stage was realized based on the double-pass nonlinear amplification construction, consisting of the PM fiber circulator, the PM fiber WDM, the 976 nm laser diode, the 0.5 m PM Yb-doped gain fiber (INO, Yb-401 PM), the PM fiber collimator, the grating pair pre-chirper (LightSmyth, 1000 lines/mm), and the grating pair compressor (LightSmyth, 1000 lines/mm). The pre-chirper was employed to manage the dispersion and the nonlinear dynamics during the double-pass nonlinear fiber amplification process. The double-pass amplified signal pulses were delivered from the PM fiber collimator, which was spliced with the output port of the PM circulator. The amplified pulses were further compressed by the compressor. The compressed high-power femtosecond signal pulses were delivered by a D-shaped mirror.

The picosecond laser delivering stage consists of the PM fiber WDM, the 976 nm laser diode, the 0.5 m PM Yb-doped gain fiber (INO, Yb-401 PM), the PM fiber collimator, and the pre-chirp managed amplifier. The pre-chirp managed amplifier was applied to further optimize the amplified picosecond pulses, consisting of the grating pair pre-chirper (LightSmyth, 1000 lines/mm), the D-shaped mirror, the PM fiber collimator, the PM fiber WDM, the 976 nm laser diode, and the 0.5 m PM Yb-doped gain fiber (INO, Yb-401 PM). The amplified picosecond signal pulses were directly delivered by the PM fiber collimator of the pre-chirp managed amplifier.

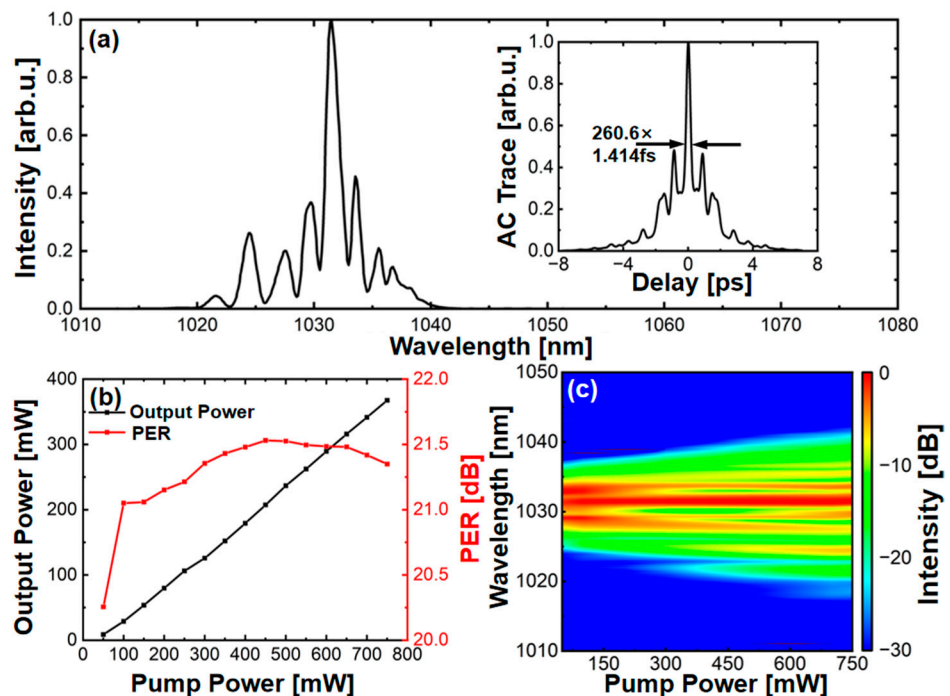
### 3. Results and Discussion

Figure 2a illustrates the optical spectra of the mode-locking signal pulses delivered by the reflection port (red curve) and the transmission port (black curve) of the NALM oscillator under a pump power of 68 mW. The corresponding full width at half maximum (FWHM) of the measured optical spectra was 1.56 nm and 4.87 nm, respectively. Figure 2b plots the measured auto-correlation traces of the delivered signal lasers. The corresponding pulse durations were 1.31 ps and 2.94 ps, respectively. Figure 2c illustrates the output powers of the delivered signal lasers as a function of injected pump power. The stable mode-locking status can be achieved under a pump power of 68 mW. Further, the NALM oscillator can lose the mode-locking state after the coupled pump power was decreased to 53 mW. Figure 2d shows the measured radio frequency (RF) spectrum of the signal laser output from the transmission port. The fundamental repetition rate of the mode-locked signal pulses was 32.77 MHz. The corresponding RF signal-to-noise ratio was 70.1 dB. The insert in Figure 2d illustrates the broadband RF spectrum with a measurement span of 1.5 GHz. The measured RF spectrum indicates the high operation stability of the mode-locking NALM laser. Compared to the material-based mode-locked laser, we realized the NALM laser with better environmental stability in the long-term operation [30].

The optical characteristics of the femtosecond laser delivering stage were carefully investigated. Figure 3a illustrates the measured optical spectrum of the amplified 1031 nm signal pulses delivered by the first-pass of the nonlinear fiber amplifier under a pump power of 750 mW. The FWHM of the output spectrum was 1.4 nm. There was no obvious Raman spectral content generated during the amplification process. The compressed auto-correlation trace of the first-pass amplified signal pulses is shown in the insert of Figure 3a. The corresponding measured pulse duration was  $260.6 \times 1.414$  fs based on the Gaussian assumption. The significant pedestals indicate the uncompressed remaining high-order phase. The corresponding output power and the polarization extinction ratio (PER) as a function of the coupled pump power are illustrated in Figure 3b. In the experiment, the output power was measured using a power meter (S314C, Thorlabs, Newton, NJ, United States) with a resolution of 5  $\mu$ W. The output power can be scaled up to 367 mW with a PER of 21.35 dB under a pump power of 750 mW. The corresponding slope efficiency was 49%. No significant amplified spontaneous emission (ASE) content was observed during the amplification process. Figure 3c illustrates the optical spectral evolution with different coupled pump powers. In order to conjugate the uncompressed high-order phase, further double-pass nonlinear pre-chirp managed amplification was implemented.



**Figure 2.** (a) The optical spectra of mode-locking pulses output from the reflection port (red curve) and the transmission port (black curve) of the NALM oscillator under a pump power of 68 mW. (b) The corresponding auto-correlation traces. (c) The output powers of the delivered signal lasers as a function of the injected pump power. (d) The radio frequency (RF) spectrum of the delivered signal laser output from the transmission port. The measured 1.5 GHz RF spectrum is plotted in the insert.



**Figure 3.** (a) The optical spectrum of the amplified signal pulses delivered by the first-pass of the femtosecond laser delivering stage under pump power of 750 mW. Insert: the corresponding auto-correlation trace of the first-pass amplified signal pulses after compression. (b) The amplified output power and the polarization extinction ratio (PER) of first-pass amplified signal pulses as a function of the launched pump power. (c) The measured spectral evolution of the first-pass amplified signal pulses delivered by the femtosecond laser delivering stage under different pump powers.

Figure 4c illustrates the optical spectrum evolution trace of the double-pass pre-chirp managed amplified pulses without optical spectral clipping under different pump powers. No significant stimulated Raman scattering (SRS) contents were observed by increasing the pump power. The optimized group delay dispersion (GDD) provided by the pre-chirper was  $-189,000 \text{ fs}^2$  at 1029 nm. The output spectrum and the measured auto-correlation trace of the double-pass amplified pulses with or without optical spectral clipping are shown in Figure 4a. The self-phase modulation (SPM) effect dominated the nonlinear process inside the double-pass nonlinear fiber amplifier. The nonlinear pedestals of the measured auto-correlation trace can be significantly inhibited by clipping the longer wavelength contents. Since the optical spectral clipper was placed between the first-pass and the second-pass of the double-pass nonlinear fiber amplifier, the spectral phase of the first-pass amplified signal pulses was optimized, after the spectral profile of the longer wavelength contents were modified with the parabolic shape [31,32]. The output power and the PER of the amplified signal pulses are illustrated in Figure 4b. The average powers of the compressed signal pulses with or without the optical spectral clipping were 171 mW and 233 mW under a pump power of 750 mW, respectively. The corresponding compressed pulse durations were  $85 \times 1.414 \text{ fs}$  and  $78 \times 1.414 \text{ fs}$ , based on the Gaussian assumption. The PER of the amplified signal pulses was reduced from 24.8 dB to 20.5 dB when the pump power increased from 50 mW to 750 mW.

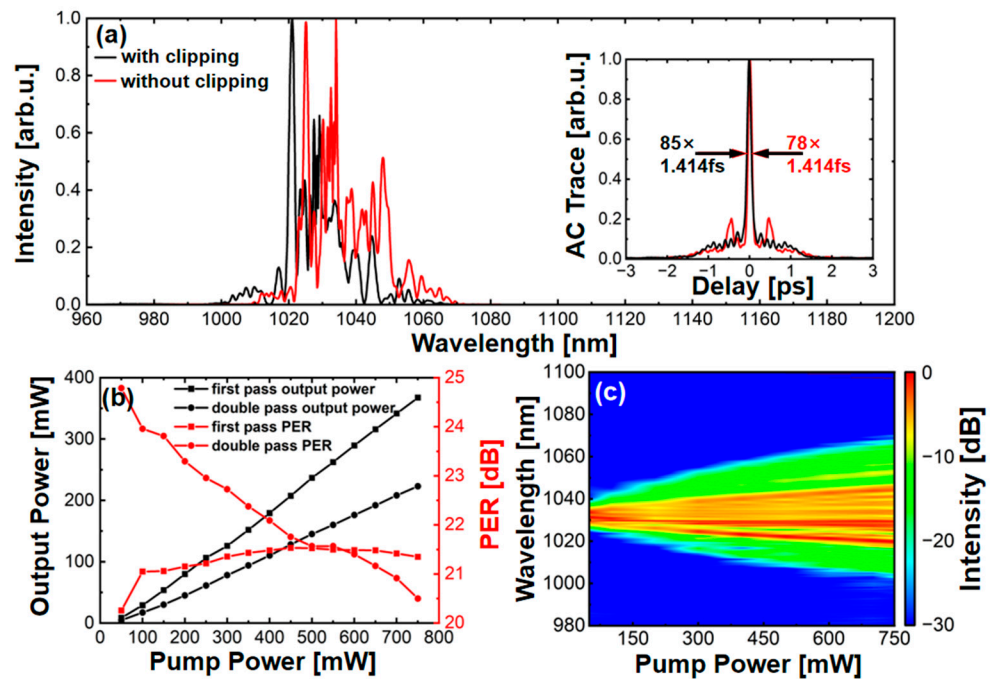


**Figure 4.** The measured optical characteristics of the amplified signal pulses with spectral clipping (black curve) and without spectral clipping (red curve) output from the femtosecond laser delivering stage. (a) The optical spectra of the amplified signal pulses delivered by the double-pass pre-chirp managed amplifier, under the pump power of 750 mW. Insert: the measured auto-correlation traces. (b) The output powers and the PER of the first-pass and double-pass amplified signal pulses as the functions of the launched pump power. (c) The spectral evolution trace of the delivered double-pass amplified signal pulses under different pump powers.

The mode-locking signal pulses delivered by the reflection port of the NALM oscillator was coupled into the single-mode fiber amplifier of the picosecond laser delivering stage. The optical spectrum of the corresponding amplified signal pulses with a coupled pump power of 120 mW is shown in Figure 5a. The measured spectral bandwidth of the 1031 nm amplified signal pulses was 4.79 nm. The insert illustrates the measured auto-correlation trace with a pulse duration of  $1.95 \times 1.414 \text{ ps}$ , based on the Gaussian assumption. The

output power of the amplified signal pulses was 27 mW under a pump power of 120 mW, as shown in Figure 5b. The PER of the amplified signal pulses was 21.5 dB under a pump power of 120 mW. The corresponding optical spectrum evolution trace of the amplified signal pulses under different pump powers is shown in Figure 5c. Further optimization of the picosecond laser delivering stage can be implemented by integrating the effects of the SPM and the negative pre-chirp to achieve the amplified signal pulses with shorter spectral bandwidth.

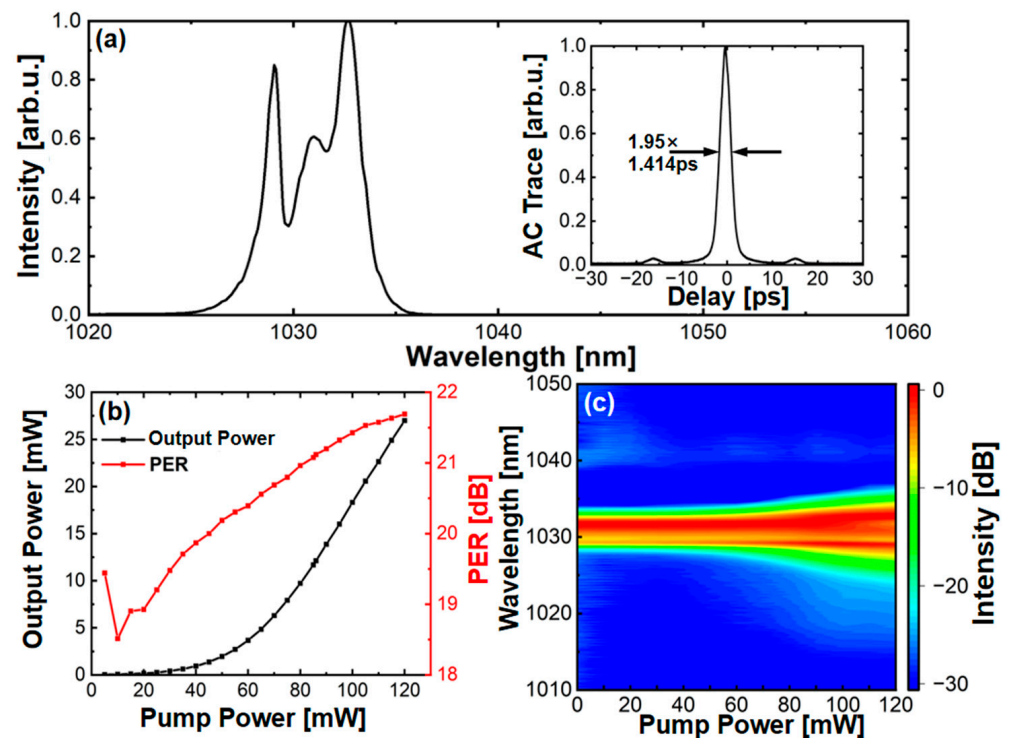


**Figure 5.** The measured optical characteristics of the amplified signal pulses output from the first-amplifier of the picosecond laser delivering stage. (a) The optical spectrum of the amplified pulses under the pump power of 120 mW. Insert: the measured auto-correlation trace. (b) The output power and the PER of the amplified signal pulses as a function of the launched pump power. (c) The spectral evolution trace of the amplified signal pulses under different pump powers.

The subsequent pre-chirp managed fiber amplifier was utilized to further optimize the amplified picosecond pulses. Figure 6a illustrates the optimized optical spectrum and the corresponding auto-correlation trace of the further nonlinear amplified signal pulses under a pump power of 800 mW. The spectral bandwidth was significantly narrowed to 1.22 nm based on the conjugation between the SPM and the  $-734,000 \text{ fs}^2@1032.5 \text{ nm}$  GDD provided by the grating pair pre-chirper of the picosecond laser delivering stage. The pulse duration of the measured auto-correlation trace was  $2.88 \times 1.414 \text{ ps}$  based on the Gaussian assumption. The output power and the PER of the amplified picosecond pulses are shown in Figure 6b. The output power of the 1032.5 nm amplified signal pulses can be scaled up to 562.5 mW. The PER of the amplified signal pulses was above 20 dB.

The measured optical power stabilities of the delivered laser pulses output from the femtosecond laser delivering stage and the picosecond laser delivering stage are shown in Figure 7. The root mean square (RMS) of the output powers of the femtosecond laser and the picosecond laser was 0.06% @ 2 h and 0.11% @ 2 h, respectively. The results indicate that the all-PM fiber front-end laser was operated with high stability.

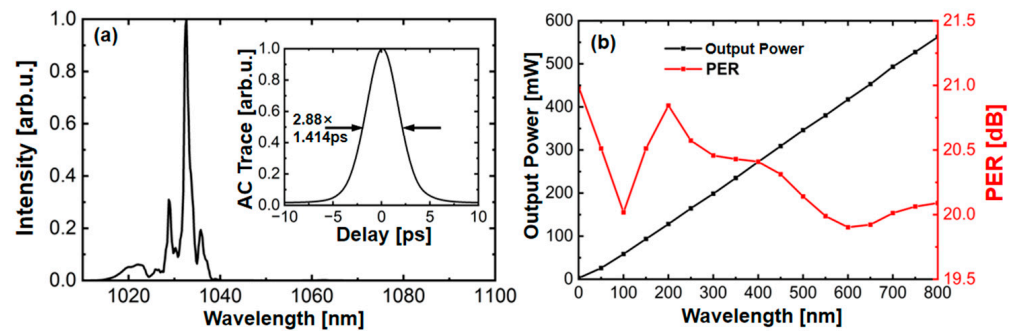


**Figure 6.** (a) Optical spectrum of the amplified pulses delivering from reflection port second-amplifier under the pump power of 800 mW. Inset: corresponding auto-correlation trace. (b) Output power and PER of second-amplified signal pulses as a function of the launched pump power.

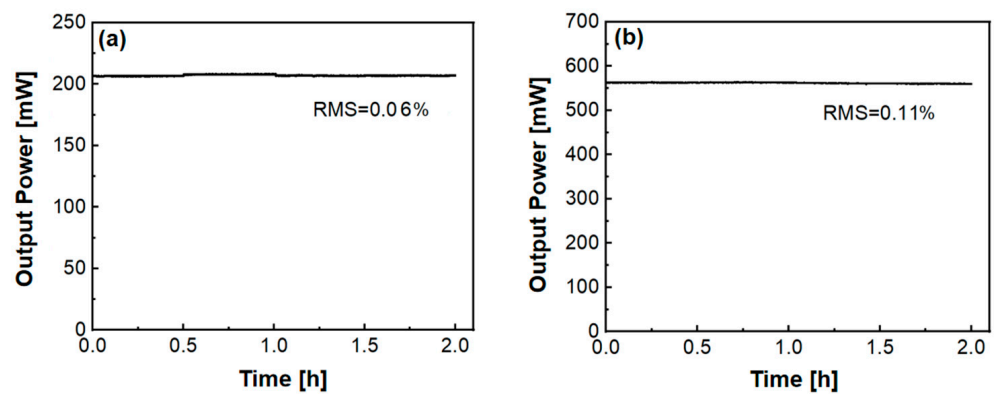


**Figure 7.** The measured optical power stability of the delivered laser pulses output from (a) the femtosecond laser delivering stage and (b) the picosecond laser delivering stage.

#### 4. Conclusions

In conclusion, we have demonstrated an all-PM fiber front-end laser delivering both the picosecond seed laser and the femtosecond seed laser based on the NALM. The 562.5 mW, 2.88 ps, 32.77 MHz, 1032.5 nm picosecond seed laser was delivered after simply amplifying the mode-locking seed laser delivered by the reflection port of the all-PM NALM laser. The 171 mW, 85 fs, 32.77 MHz, 1029 nm femtosecond seed laser was realized, utilizing double-pass nonlinear amplification. The corresponding PER of the amplified picosecond seed laser and femtosecond seed laser was above 20 dB. The corresponding root mean square (RMS) of the attenuated output powers of the picosecond seed laser and the femtosecond seed laser was 0.11% and 0.06%. The experimental results indicate that this stable all-PM fiber front-end laser can satisfy the urgent requirements of the aforementioned state-of-the-art applications [17–22].

**Author Contributions:** Conceptualization, Y.Z. and Y.L.; methodology, Y.L.; software, Y.Z.; validation, Y.Z., H.Z. and K.G.; investigation, Y.Z. and K.G.; resources, Y.L.; data curation, Y.Z. and H.Z.; writing—original draft, Y.Z.; writing—review and editing, W.Q., T.F., X.Z. and Y.L.; visualization, Y.Z.; supervision, Y.L. All authors have read and agreed to the published version of the manuscript.

**Funding:** This research was funded by the Natural Science Foundation of Shandong Province (ZR2021QF054).

**Institutional Review Board Statement:** No applicable.

**Informed Consent Statement:** No applicable.

**Data Availability Statement:** Data underlying the results presented in this paper are not publicly available at this time but may be obtained from the authors upon reasonable request.

**Conflicts of Interest:** The authors declare no conflict of interest.

## References

1. Hoover, E.; Squier, J. Advances in multiphoton microscopy technology. *Nat. Photonics* **2013**, *7*, 93–101. [[CrossRef](#)] [[PubMed](#)]
2. Liu, W.; Chia, S.H.; Chung, H.Y.; Greinert, R.; Kärtner, F.; Chang, G. Energetic ultrafast fiber laser sources tunable in 1030–1215 nm for deep tissue multi-photon microscopy. *Opt. Express* **2017**, *25*, 6822–6831. [[CrossRef](#)] [[PubMed](#)]
3. Zhao, Y.; Guo, P.; Li, X.; Jin, Z. Ultrafast photonics application of graphdiyne in the optical communication region. *Carbon* **2019**, *149*, 336–341. [[CrossRef](#)]
4. Horowitz, M.; Menyuk, C.R.; Carruthers, T.F.; Duling, I.N. Theoretical and experimental study of harmonically modelocked fiber lasers for optical communication systems. *J. Lightw. Technol.* **2000**, *18*, 1565–1574. [[CrossRef](#)]
5. Kongas, J.; Amberla, T.; Rekow, M. Metal Micromachining with a New High Average Power Picosecond Pulse Fiber Laser. In Proceedings of the International Congress on Applications of Lasers and Electro-Optics, Wuhan, China, 23–25 March 2006.
6. Shah, L.; Fermann, M.; Dawson, J.; Barty, C. Micromachining with a 50 W, 50  $\mu$ J, sub-picosecond fiber laser system. *Opt. Express* **2006**, *14*, 12546–12551. [[CrossRef](#)]
7. Lee, K.; Ding, X.; Hammond, T.J.; Fermann, M.E.; Vampa, G.; Corkum, P.B. Harmonic generation in solids with direct fiber laser pumping. *Opt. Lett.* **2017**, *42*, 1113–1116. [[CrossRef](#)]
8. Zhao, Z.; Kobayashi, Y. Realization of a mW-level 10.7-eV ( $\lambda = 115.6$  nm) laser by cascaded third harmonic generation of a Yb: fiber CPA laser at 1-MHz. *Opt. Express* **2017**, *25*, 13517–13526. [[CrossRef](#)]
9. Guan, M.; Chen, D.; Hu, S.; Zhao, H.; You, P.; Meng, S. Theoretical Insights into Ultrafast Dynamics in Quantum Materials. *Ultrafast Sci.* **2022**, *2022*, 9767251. [[CrossRef](#)]
10. Zhang, Z.; Zhang, J.; Chen, Y.; Xia, T.; Wang, L.; Han, B.; He, F.; Sheng, Z.; Zhang, J. Bessel Terahertz Pulses from Superluminal Laser Plasma Filaments. *Ultrafast Sci.* **2022**, *2022*, 9870325. [[CrossRef](#)]
11. Liu, X.; Yao, X.; Cui, Y. Real-Time Observation of the Buildup of Soliton Molecules. *Phys. Rev. Lett.* **2018**, *121*, 023905. [[CrossRef](#)]
12. Liu, X.; Pang, M. Revealing the Buildup Dynamics of Harmonic Mode-Locking States in Ultrafast Lasers. *Laser Photonics Rev.* **2019**, *13*, 1800333. [[CrossRef](#)]
13. Liu, X.; Popa, D.; Akhmediev, N. Revealing the Transition Dynamics from Q Switching to Mode Locking in a Soliton Laser. *Phys. Rev. Lett.* **2019**, *123*, 093901. [[CrossRef](#)] [[PubMed](#)]
14. Li, C.; Ma, Y.; Gao, X.; Niu, F.; Jiang, T.; Wang, A.; Zhang, Z. 1 GHz repetition rate femtosecond Yb: fiber laser for direct generation of carrier-envelope offset frequency. *Appl. Opt.* **2015**, *54*, 8350–8353. [[CrossRef](#)]
15. Liu, Z.; Ziegler, Z.; Wright, L.; Wise, F. Megawatt peak power from a Mamyshev oscillator. *Optica* **2017**, *4*, 649–654. [[CrossRef](#)] [[PubMed](#)]
16. Song, Y.; Hu, M.; Gu, C.; Chai, L.; Wang, C.; Zheltikov, A.M. Mode-locked Yb-doped large-mode-area photonic crystal fiber laser operating in the vicinity of zero cavity dispersion. *Laser Phys. Lett.* **2010**, *7*, 230–235. [[CrossRef](#)]
17. Zhu, Q.; Zhou, K.; Su, J.; Xie, N.; Huang, X.; Zeng, X.; Wang, X.; Wang, X.; Zuo, Y.; Jiang, D.; et al. The Xingguang-III laser facility: Precise synchronization with femtosecond, picosecond and nanosecond beams. *Laser Phys. Lett.* **2017**, *15*, 015301. [[CrossRef](#)]
18. Wu, Y.; Zhu, B.; Dong, K.; Lu, F.; He, S.; Zhang, B.; Yan, Y.; Yu, M.; Tan, F.; Wang, S.; et al. XingGuang III laser facility and its experimental ability to drive high-energy particle beams. *Laser Phys.* **2020**, *30*, 096001. [[CrossRef](#)]
19. Cavalieri, A.; Fritz, D.; Lee, S.; Bucksbaum, P.; Reis, D.; Rudati, J.; Mills, D.; Fuoss, P.; Stephenson, G.; Kao, C.; et al. Clocking femtosecond X rays. *Phys. Rev. Lett.* **2005**, *94*, 114801. [[CrossRef](#)]
20. Damerau, H. CERN: Timing, Synchronization & Longitudinal Aspects. *CERN Yellow Rep. School Proc.* **2018**, *5*, 163.
21. Papadopoulos, D.N.; Ramirez, P.; Genevri, K.; Ranc, L.; Lebas, N.; Pellegrina, A.; Le Blanc, C.; Monot, P.; Martin, L.; Zou, J.P.; et al. High-contrast 10 fs OPCPA-based front end for multi-PW laser chains. *Opt. Lett.* **2017**, *42*, 3530–3533. [[CrossRef](#)]
22. Puppini, M.; Deng, Y.; Prochnow, O.; Ahrens, J.; Binhammer, T.; Morgner, U.; Krenz, M.; Wolf, M.; Ernstorfer, R. 500 kHz OPCPA delivering tunable sub-20 fs pulses with 15 W average power based on an all-ytterbium laser. *Opt. Express* **2015**, *23*, 1491–1497. [[CrossRef](#)]
23. Khagai, A.; Melkumov, M.; Riumkin, K.; Khopin, V.; Firstov, S.; Dianov, E. NALM-based bismuth-doped fiber laser at 1.7  $\mu$ m. *Opt. Lett.* **2018**, *43*, 1127–1130. [[CrossRef](#)] [[PubMed](#)]
24. Smirnov, S.; Kobtsev, S.; Ivanenko, A.; Kokhanovskiy, A.; Kemmer, A.; Gervaziev, M. Layout of NALM fiber laser with adjustable peak power of generated pulses. *Opt. Lett.* **2017**, *42*, 1732–1735. [[CrossRef](#)]
25. Yu, Y.; Teng, H.; Wang, H.; Wang, L.; Zhu, J.; Fang, S.; Chang, G.; Wang, J.; Wei, Z. Highly-stable mode-locked PM Yb-fiber laser with 10 nJ in 93-fs at 6 MHz using NALM. *Opt. Express* **2018**, *26*, 10428–10434. [[CrossRef](#)] [[PubMed](#)]
26. Liu, G.; Wang, A.; Zhang, Z. 84-fs 500-MHz Yb: Fiber-Based Laser Oscillator Mode Locked by Biased NALM. *IEEE Photonics Technol. Lett.* **2017**, *29*, 2055–2058. [[CrossRef](#)]
27. Gao, W.; Liu, G.; Zhang, Z. 44.6 fs pulses from a 257 MHz Er: fiber laser mode-locked by biased NALM. *Chin. Opt. Lett.* **2018**, *16*, 111401.
28. Chong, A.; Renninger, W.; Wise, F. All-normal-dispersion femtosecond fiber laser with pulse energy above 20 nJ. *Opt. Lett.* **2007**, *32*, 2408–2410. [[CrossRef](#)] [[PubMed](#)]
29. Aguergaray, C.; Hawker, R.; Runge, A.; Erkintalo, M.; Broderick, N. 120 fs, 4.2 nJ pulses from an all-normal-dispersion, polarization-maintaining, fiber laser. *Appl. Phys. Lett.* **2013**, *103*, 121111. [[CrossRef](#)]
30. Zhang, C.; Liu, J.; Gao, Y.X.; Li, X.; Lu, H.; Wang, Y.; Feng, J.; Lu, J.; Ma, K.; Chen, X. Porous nickel oxide micron polyhedral particles for high-performance ultrafast photonics. *Opt. Laser Technol.* **2022**, *146*, 107546. [[CrossRef](#)]

31. Schimpf, D.; Limpert, J.; Tünnermann, A. Controlling the influence of SPM in fiber-based chirped-pulse amplification systems by using an actively shaped parabolic spectrum. *Opt. Express* **2007**, *15*, 16945–16953. [[CrossRef](#)]
32. Song, H.; Liu, B.; Chen, W.; Li, Y.; Song, Y.; Wang, S.; Chai, L.; Wang, C.; Hu, M. Femtosecond laser pulse generation with self-similar amplification of picosecond laser pulses. *Opt. Express* **2018**, *26*, 26411–26421. [[CrossRef](#)] [[PubMed](#)]

**Disclaimer/Publisher’s Note:** The statements, opinions and data contained in all publications are solely those of the individual author(s) and contributor(s) and not of MDPI and/or the editor(s). MDPI and/or the editor(s) disclaim responsibility for any injury to people or property resulting from any ideas, methods, instructions or products referred to in the content.